POSTCRACK SCALING RELATIONS FOR FIBER REINFORCED CEMENTITIOUS COMPOSITES

By Victor C. Li,[1] Member, ASCE

ABSTRACT: The prepeak and postpeak stress-displacement relations are derived for the bridging mechanism associated with randomly oriented discontinuous flexible fibers in cement-based composites. The postcrack strength and fracture energy are examined in light of the scaling micromechanical parameters, including fiber snubbing coefficient, diameter, aspect ratio, volume fraction, and interface bond strength. Comparisons of theoretically derived postcracking stress-displacement relation and pullout fracture energy with experimental data of both steel-fiber and synthetic-fiber reinforced cementitious composites of widely varying micromechanical parametric values suggest that the simple model approximates the bridging behavior in this type of composite.

INTRODUCTION

Introduction of fibers in a cementitious composite stabilizes microcracks in the matrix. When microcracks are adequately suppressed from propagation, a pseudostrain-hardening behavior occurs, reflecting the opening of microcracks distributed over the volume of the body. This type of pseudostrain-hardening behavior in brittle matrix composites is reminiscent of the strain-hardening behavior in metals, where the origin of strain hardening is associated with the activation of dislocations and their stabilization due to entanglement or pinning. A direct benefit of the pseudostrain-hardening behavior in fiber reinforced cementitious composites (FRCC) is the increase of critical strain at the first cracking stress, typically defined as the load at which a certain critical crack enlarges across the complete cross section of the specimen. Due to energetic reasons, the composite critical strain can be substantially larger than the matrix critical strain, if properly reinforced. Increased critical strain enables the material to tolerate larger amounts of deformation without visible cracking.

If, after first cracking, the fiber and the fiber/matrix interface are both strong enough to carry the load shed by the matrix, it is possible to induce what is known as multiple cracking. This happens when the bridging fibers across the first crack can continue to increase with increase crack opening, causing other microcracks to spread and form multiple subparallel fracture planes of the specimen. Multiple cracking is yet another form of psuedostrain hardening, although the cracks formed are usually large enough not to be rehealed, and the material then suffers permanent damage.

After multiple cracking, the load is fully born by the fibers, and either fiber breakage or pullout occurs. For composites with low fiber volume fractions, this happens immediately following first crack, with no multiple cracking. Because fiber pullout can be accompanied by significant amount of energy absorption due to interface frictional work, the fracture energy

[1]Assoc. Prof., Advanced Civ. Engrg. Materials Res. Lab., Dept. of Civ. and Envirn. Engrg., Univ. of Michigan, Ann Arbor, MI 48109-2125.

Note. Discussion open until July 1, 1992. To extend the closing date one month, a written request must be filed with the ASCE Manager of Journals. The manuscript for this paper was submitted for review and possible publication on December 26, 1990. This paper is part of the ***Journal of Materials in Civil Engineering***, Vol. 4, No. 1, February, 1992. ©ASCE, ISSN 0899-1561/92/0001-0041/$1.00 + $.15 per page. Paper No. 1174.

of the composite can be greatly improved. Fiber pullout in FRCC has been demonstrated by a number of researchers.

One of the early demonstrations of the existence of pseudostrain hardening in the form of increased critical strain and multiple cracking can be found in the now-classic paper by Aveston et al. (1971), which contains both theoretical and experimental results. Interest in this class of "high-performance cement-based composites" has been renewed in recent years. The newer literature (e.g., Bache 1987; Krenchel and Stang 1989; Shah 1990) on this subject embodies novel processing and advanced imaging technology. Examples of fracture energy increase due to fiber pullout can be found in many publications [see, e.g., Wecharatana and Shah (1983), for steel FRCC; and Li and Ward (1989), for polymeric FRCC].

The existence of the aforementioned phenomena is largely controlled by the collective behavior of fibers bridging across a matrix crack that opens in response to remote load. For convenience, we shall call the varying smeared traction across the opening crack the bridging stress-displacement curve. The rising part of the bridging stress-displacement curve is mainly associated with the delamination process of the fiber/matrix interface. While this prepeak part of the curve plays a significant role in governing the magnitude of the first crack strength, the existence of steady state first-crack strength [see, e.g. Li (1990); Li and Leung (1991)], and the presence or absence of multiple cracking, it is unfortunately not directly measurable. What is measurable at this prepeak loading stage is the composite tensile property jointly governed by this prepeak stress-displacement curve and the matrix fracture properties. After composite peak strength, however, the postpeak bridging stress-displacement curve is directly measured in the composite test, since at this stage, only the fiber (and the interface) determines the composite behavior.

This paper presents a theoretical study of the complete (both the ascending and descending branches) bridging stress-displacement curve (hereafter called the σ_B-δ curve) of randomly distributed discontinuous fiber reinforced cementitious composites. By adopting some simplifying assumptions, closed-form analytic solutions are derived based on which the scaling laws of the bridging stress-displacement curve and composite fracture energy are examined with respect to fiber, matrix, and fiber/matrix interaction (includes both interface and snubbing, to be discussed later) properties. Comparisons with experimental data of the postpeak stress-displacement curves and with composite fracture energy (Visalvanich and Naaman, 1982) for steel FRCC are also given. Recent data on a polymeric FRCC by Wang et al. (1990) are likewise shown to be well described by the same scaling laws proposed here.

Prepeak Bridging Stress-Displacement Curve

Consider an isolated fiber loaded at its end with a force P resisted by a constant frictional bond τ at its interface along its length ℓ embedded in concrete. By ignoring the elastic bond, the length of the slip activated zone where τ acts on can be calculated based on simple force equilibrium. As the load P increases, extension of this slip zone occurs. This is generally described as "debonding" but should be understood as the activation of frictional slip. Displacement δ of the fiber-loaded end also increases as a result of the stretching of the fiber segment along the length of the slip zone. The relationship between P and δ may be derived and is given by

$$P(\delta) = \pi\sqrt{\frac{E_f d_f^3 \tau \delta}{2}} \quad \text{for } \delta \le \delta_0 \qquad (1)$$

where d_f and E_f = the fiber diameter and elastic modulus; and $\delta_0 \equiv 2\ell^2\tau/E_f d_f$ corresponds to the displacement δ at which debonding is completed along the full length of the embedded fiber segment. Appendix I shows that (1), derivable by assuming a linear stress distribution along the debonded segment of the fiber, is a good approximation provided that $(\ell/d_f)/(E_f/\tau)$ is much smaller than unity.

After debonding reaches the embedded end without rupture, fiber pullout proceeds and the pullout load decreases. Again, assuming a constant frictional bond and ignoring the elastic stretching of the fiber at this stage, the pullout force is related to the load point displacement through

$$P(\delta) = \pi\tau\ell d_f\left[1 - \frac{(\delta - \delta_0)}{\ell}\right] \quad \text{for } \ell \ge \delta > \delta_0 \qquad (2)$$

Fig. 1 shows the P-δ relationship for fibers of various embedment lengths. For some fibers, where the interfacial slip resistance depends on the amount of sliding, (2) would be a gross simplification, and the more detailed analysis of Li et al. (1991) is recommended.

Eqs. (1) and (2) are for fibers pulled out in a direction along the fiber axis. For nonaligned fibers, which is often the case in randomly distributed discontinuous FRCC, various studies have indicated an angle effect on the pullout load P. For flexible (in bending, dependent on elastic stiffness and fiber diameter) steel and polymeric fibers, Morton and Groves (1976) and Li et al. (1990b) found an increase of P with angle ϕ of inclination of fiber to the loading axis. This snubbing effect could be incorporated into the pullout force by recognizing

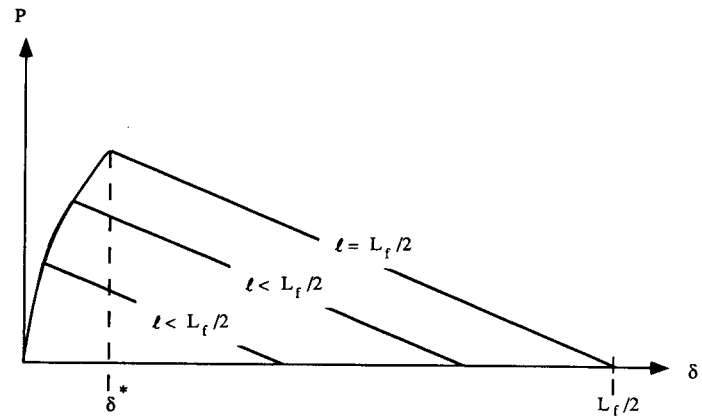

FIG. 1. Schematics of Single Fiber Pullout Force P versus Pullout Displacement δ Relation, for Various Embedded Fiber Lengths ℓ. δ^* Corresponds to Pullout Displacement at Peak Load of Fiber with Embedded Length Equal to Half Fiber Length

$$P(\delta;\phi) = P(\delta;\phi = 0)e^{f\phi} \quad \ldots\ldots (3)$$

as originally suggested by Morton and Groves, where f is a snubbing coefficient. Experimental tests of fiber pullout at inclined angles up to 80° suggest f-values of 0.7 and 0.9 for nylon and polypropylene fibers embedded in a normal-strength mortar matrix. It may be expected, however, that matrix yielding or spalling at high fiber angles would tend to limit the snubbing effect as described in (3).

For a composite with fiber volume fraction V_f, Li et al. (1991) showed that the composite σ_B-δ curve can be predicted by integrating over the contributions of (only) those individual fibers that cross the matrix crack plane:

$$\sigma_B(\delta) = \frac{4V_f}{\pi d_f^2}\int_{\phi=0}^{\pi/2}\int_{z=0}^{(L_f/2)\cos\phi} P(\delta)p(\phi)p(z)\,dz\,d\phi \quad \ldots\ldots (4)$$

where $p(\phi)$ and $p(z)$ = probability density functions of the orientation angle and centroidal distance of fibers from the crack plane. For uniform random distributions, $p(\phi) = \sin\phi$, and $p(z) = 2/L_f$ (Li et al. 1991).

Using (1)–(3) in (4), we find (Appendix II), in normalized form:

$$\tilde{\sigma}_B(\tilde{\delta}) = g\left[2\left(\frac{\tilde{\delta}}{\tilde{\delta}^*}\right)^{1/2} - \frac{\tilde{\delta}}{\tilde{\delta}^*}\right] \qquad \text{for } \tilde{\delta} \le \tilde{\delta}^* \quad \ldots\ldots (5)$$

where $\tilde{\sigma}_B \equiv \sigma_B/\sigma_0$, $\sigma_0 \equiv V_f\tau(L_f/d_f)/2$, and $\tilde{\delta} \equiv \delta/(L_f/2)$. $\tilde{\delta}^* \equiv (\tau/E_f)(L_f/d_f)$ corresponds to the maximum attainable (normalized by $L_f/2$) value of δ_0 for the fiber with the longest embedment length of $L_f/2$. The snubbing factor g is defined in terms of the snubbing coefficient f:

$$g \equiv \frac{2}{4 + f^2}(1 + e^{\pi f/2}) \quad \ldots\ldots (6)$$

For f between 0 and 1, g ranges from 1 to 2.32, as shown in Fig. 2. Eq. (5) is used to compute the prepeak part of the σ_B-δ curve, Fig. 3(a), for various snubbing coefficient magnitudes. In general, the peaks of the σ_B-δ curves occur slightly prior to δ^*. For $\delta^* << 1$, the maximum bridging stress approximately scales with $g\sigma_0$. This also corresponds to the highest value in the postpeak stress-displacement curve, as shown herein. As discussed in

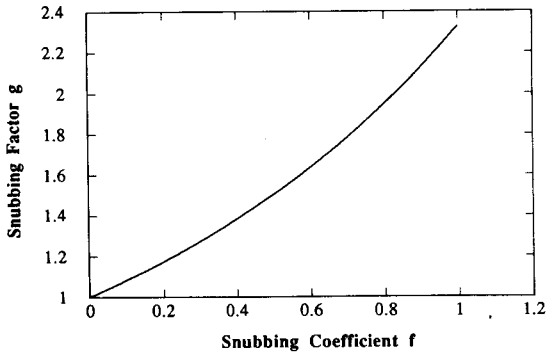

FIG. 2. Relationship between Snubbing Factor g to Snubbing Coefficient f

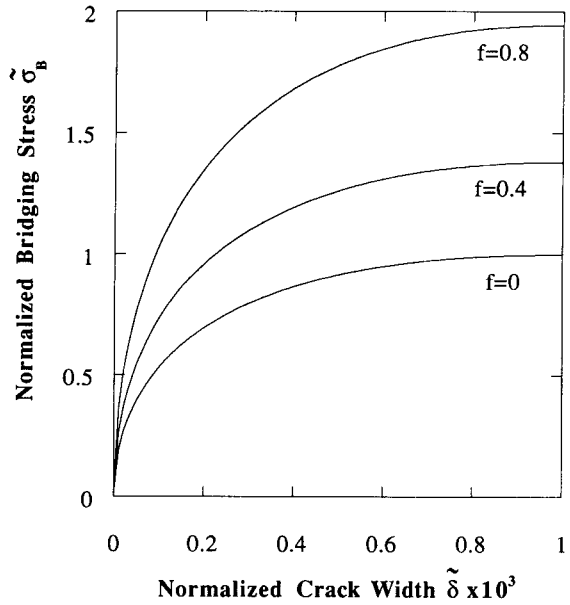

FIG. 3(a). Relationship between Normalized Bridging Stress and Normalized Crack Width for Three Different Values of Snubbing Factor and for Prepeak

Li (1990) and Li and Leung (1991), this maximum bridging stress controls the existence of steady state first cracking and hence the reliability of material. The higher this value is, the higher the first crack strength is and the more reliable the material becomes. From this point of view, it is preferable to have large values of f, V_f, τ, and L_f/d_f. This is likely to be the case in composites like asbestos cement. However, these parameters, which lead to high bridging stress, also induce the possibility of fiber rupture, and eliminate any possibility of energy absorption through fiber pullout.

Postpeak Bridging Stress-Displacement Relation

The postpeak stress-displacement curve can be obtained from (3) and (4). Full derivation is given in Appendix III. The result is:

$$\tilde{\sigma}_B(\tilde{\delta}) = g(1 - \tilde{\delta})^2 \qquad \text{for } 1 > \tilde{\delta} > \tilde{\delta}^* \quad \ldots\ldots (7)$$

where additional terms involving $\tilde{\delta}^*$ and higher orders have been neglected, suitable for the case when $\tilde{\delta}^* << 1$. Eq. (7) is used to compute the postpeak part of the σ_B-δ curve, Fig. 3(b) [note different scales for the crack width between Figs. 3(a) and 3(b)], for various snubbing coefficients. It is interesting to compare (7) with the semiempirically derived expression for the postpeak stress-displacement curve of Visalvanich and Naaman (1982):

$$\frac{\sigma_B(\tilde{\delta})}{\alpha\tau V_f\left(\frac{L_f}{d_f}\right)} = (0.1\tilde{\delta} + 1)(1 - \tilde{\delta})^2 \quad \ldots\ldots (8)$$

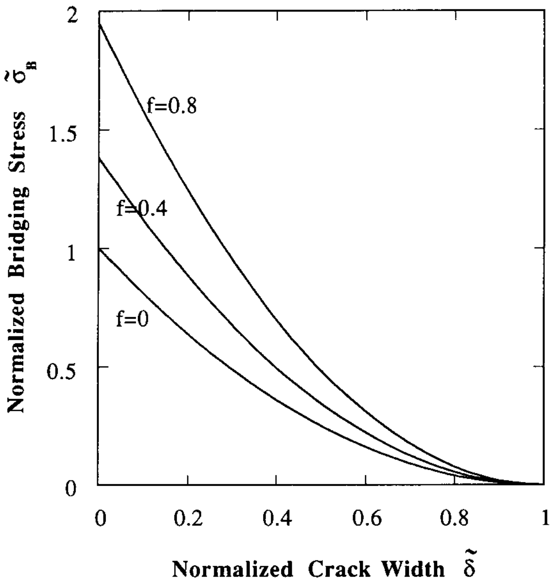

FIG. 3(*b*). Relationship between Normalized Bridging Stress and Normalized Crack Width for Three Different Values of Snubbing Factor and for Postpeak

where α = an efficiency factor related to the random distribution and discontinuous nature of the fibers. In their analysis, the snubbing effect is not considered, so that if the experimental data reflects this effect, it would be incorporated into the factor α. The term $0.1\tilde{\delta} + 1$ in (8) does not differ much from unity especially when the typical amount of scatter in experimental data is taken into consideration. Thus the dependence on crack-opening displacement of the bridging stress is expressed through the $(1 - \tilde{\delta})^2$ term in both (7) and (8). Indeed, Wecharantana and Shah (1983) arrived at exactly the same $(1 - \tilde{\delta})^2$ dependence through empirical fit of steel FRCC data of Naaman et al. (1974) and Shah et al. (1978). (One set of Visalvanich and Naaman's data was also employed in the study of Wecharantana and Shah.) Unlike (8), where this dependence has been obtained through a curve-fitting procedure to experimental data, (7) has been derived from the consideration of the sum total contribution of individual fibers undergoing slippage as expressed in (2) and (4). Furthermore, the multiplying factor α is now explicitly expressed as $g/2$, without any ambiguity of its origin. A similar form of (7) has been previously derived by Cotterell and Mai (1988), based on a consideration of "efficiency factor" and expected number of bridging fibers, although the mechanism of snubbing is not considered there (and probably could not be included in such a formulation).

As discussed earlier, the maximum value σ_{pc} of the bridging stress-displacement curve, often referred to as the composite postcrack strength, scales with $g\sigma_0$, which may be obtained from (7) by setting $\tilde{\delta}$ to zero. That is

$$\sigma_{pc} = \frac{1}{2} g\tau V_f \left(\frac{L_f}{d_f}\right) \quad \text{.......... (9)}$$

Eq. (9) has also derived by Aveston et al. (1974) for the case when the snubbing effect is absent (i.e., when $g = 1$). When σ_{pc}/τ is plotted against the reinforcement index $\frac{1}{2}V_f(L_f/d_f)$, the result should be a straight line with slope given by g. This is shown in Fig. 4, which employs data for steel fiber reinforced mortar, as well as data for spectra (a high-modulus polyethylene) reinforced normal- and high-strength mortar (Wang et al. 1990). The normalizing values of τ for steel/mortar interface is chosen as 4 MPa [within typical experimentally determined range, see, e.g., Bentur and Mindess (1990) and 1 MPa for the spectra fiber/mortar interface [measured values, Li et al. (1990b)]. Fig. 4 suggests that for the steel fiber reinforced mortar, a snubbing friction f of close to unity describes the data well, whereas f is approximately 0.55 for both spectra/normal-strength mortar and spectra/high-strength mortar. In contrast, limited data of direct pullout test of nylon fiber indicate higher value of f in high-strength mortar compared to that in normal-strength mortar (Li et al. 1990b). The value of f for spectra fiber should be interpreted with caution due to the limited data points and the large standard deviation in the data for spectra reinforced normal-strength mortar. The original data shows significant fluctuations in the postcrack loads, especially near the peak, presumably due to matrix spalling effects. These fluctuations impose substantial uncertainty in the value of σ_{pc}, and

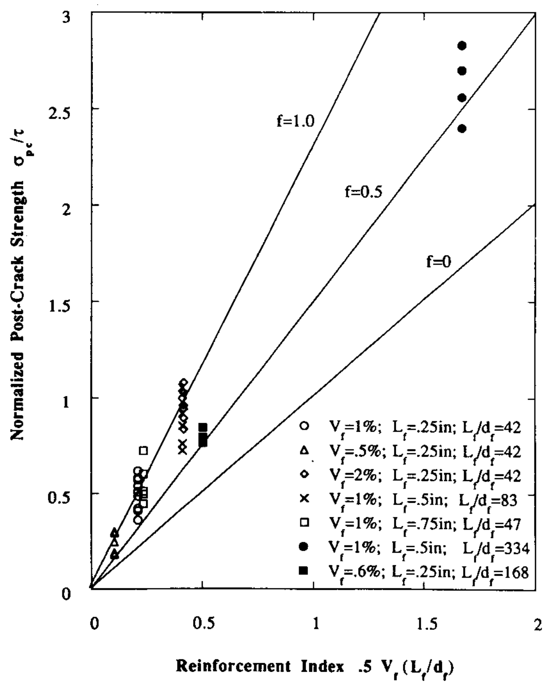

FIG. 4. Normalized Postcrack Strength Plotted Against Reinforcement Index for Data from Both Steel and Spectra Fibers. Straight Lines are Based on (9). [Steel Fiber Composite Data from Visalvanich and Naaman (1982); Spectra Fiber Composite Data from Wang et al. (1990)]

hence the value of f. The accuracy of f is also subject to error in the value of τ employed.

With the value of τ and f chosen, it is possible to plot the $\bar{\sigma}_B/g$ versus $\tilde{\delta}$, using the five sets of data given by Visalvanich and Naaman (1982) for steel fiber reinforced mortar. This is shown in Fig. 5, together with the theoretical curve of (7). The good fit is not surprising, given the excellent match between (7) and (8), the latter of which has been obtained semiempirically. Each point in each set of data shown in Fig. 5 represents an average of at least five repeated tests. A similar comparison is shown in Fig. 6 for the spectra composites mentioned previously. Each line represents an average of five tests for the FRCC with the normal-strength mortar matrix and three tests for that with the high-strength mortar matrix.

Composite Fracture Energy

The fracture energy due to fiber pullout can be computed from

$$G_c = \int_0^{L_f/2} \sigma_B(\delta)\, d\delta \quad \ldots\ldots (10)$$

and with σ_B given by (7), it can be shown that

$$G_c = \frac{1}{12} g\tau V_f d_f \left(\frac{L_f}{d_f}\right)^2 \quad \ldots\ldots (11)$$

This result is a specialized case of that given by Li et al. (1991), who also

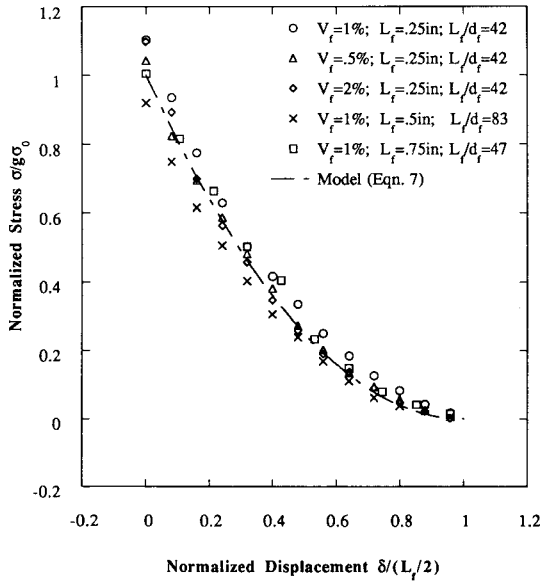

FIG. 5. Comparison of Theoretically and Experimentally Determined Normalized Postpeak Stress-Displacement Curves for Steel Fiber Reinforced Cementitious Composites [Data from Visalvanich and Naaman (1982)]

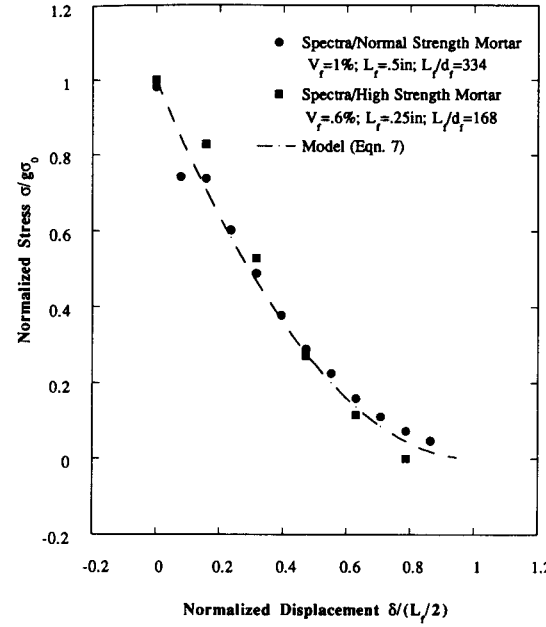

FIG. 6. Comparison of Theoretically and Experimentally Determined Normalized Postpeak Stress-Displacement Curves for Spectra Fiber Reinforced Cementitious Composites [Data from Wang et al. (1990)]

consider the effect of fiber rupture on G_c. Comparison with the "work of fracture" study on discontinuous aligned fiber composites of Cooper and Kelly (1970) reveals that the random distribution of fibers reduces the fracture energy by a factor of two, if there is no snubbing effect, i.e., if $g = 1$ corresponding to $f = 0$.

Energy is absorbed in the debonding process. This part of the fracture energy may be estimated by integrating the prepeak stress-displacement curve (5) with respect to δ up to δ^*. The result is

$$G_r = \frac{5}{12} g\tau V_f d_f \left(\frac{L_f}{d_f}\right)^2 \delta^* \quad \ldots\ldots (12)$$

Comparison with (11) indicates that this part of the fracture energy is negligibly small, of the order of δ^* of the postpeak pullout fracture energy.

Eq. (11) suggests that the fracture energy scales with the square of fiber length, as for the case of aligned fiber composites, assuming no fiber rupture occurs. In the studies by Visalvanich and Naaman (1982) and Wang et al. (1990), this assumption seems to be justified as they reported the dominant mode of failure being fiber pullout. Fig. 7 shows a plot of normalized G_c against (L_f/d_f) for the data given by Visalvanich and Naaman for steel fiber reinforced mortar. The theoretical curve of (11) is also shown. To include the spectra fiber reinforced mortar data, we replot Fig. 7 on a log-log scale such that the slope of the line $\log[G_c/(gV_f d_f \tau/12)]$ versus $\log[L_f/d_f]$ should have a value of 2, according to (11). This is shown in Fig. 8, together with the experimental data for both steel and spectra fiber composites.

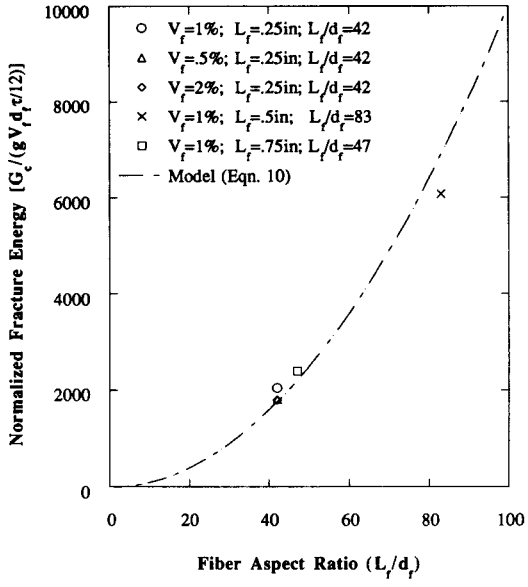

FIG. 7. Comparison of Theoretically and Experimentally Determined Normalized Fracture Energy for Steel Fiber Reinforced Cementitious Composites [Data from Visalvanich and Naaman (1982)]

Further Analyses and Concluding Remarks

The prepeak stress-displacement curve, the postpeak stress-displacement curve, and their corresponding fracture energy associated with the interface delamination and pullout processes are analyzed for discontinuous flexible fiber reinforced cementitious composites. The scaling laws for each of these quantities are given in terms of measurable fiber, matrix, interface, and snubbing parameters. Comparisons with experimental data for steel fiber and spectra fiber reinforced cementitious composites appear to confirm the validity of the theoretical treatment.

The postcrack strength [(9)] and the fracture energy [(11)] both scale with $g\tau$. This suggests that the snubbing factor may be regarded as an effective enhancement of the bond strength. For fibers with length less than the critical length, this synergism between snubbing and interface bond does increase the postcrack strength and the fracture energy. This combined multiplicative (as opposed to additive) effect could be taken advantage of when inadequate fiber/matrix bonding occurs, or when fiber lengths are limited by processing requirements to length much below the critical length. However, the optimal fiber length is given by

$$L_{op} \approx \frac{d_f \sigma_f}{4g\tau} \quad \ldots\ldots (13)$$

so that the optimal fracture energy is

$$G_{op} \approx \frac{1}{48} \frac{V_f d_f \sigma_f^2}{g\tau} \quad \ldots\ldots (14)$$

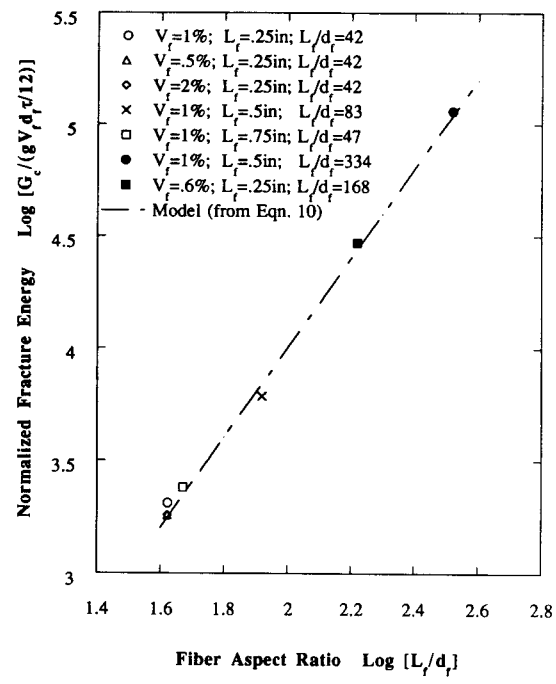

FIG. 8. Comparison of Theoretically and Experimentally Determined Normalized Fracture Energy for Spectra Fiber Reinforced Cementitious Composites [Data from Wang et al. (1990)]

Eqs. (9) and (14) indicate that $g\tau$ becomes now a tradeoff parameter between postcrack strength and optimal fracture energy. This means that if postcrack strength needs to be optimized when designing for pseudostrain hardening, for example, then a high $g\tau$ is desirable. However, this will reduce the optimal fracture energy as expressed in (14), due to increasing amount of fiber rupture. A detail analysis of the fracture energy, where fiber pullout and fiber rupture can simultaneously occur, is given in Li et al. (1991).

It is interesting to note that the optimal fracture energy scales with the fiber diameter, whereas the postcrack strength scales inversely with the fiber diameter. This implies that small fiber diameter is desirable for pseudostrain hardening, whereas large fiber diameter is desirable for high energy absorption.

For composites where the ultimate tensile strength is higher than the postcrack strength, there is a possibility of an underestimation of σ_{pc} of the bridging stress-displacement curve. This can be illustrated schematically for the FRCC specimen in Fig. 9. Three stages of progressive uniaxial loading are shown. Their corresponding stages of bridging stress displacement at the midcrack point and of the measured composite stress-deformation curves, are also indicated in Fig. 10. Two scenarios are possible. In the first scenario [Fig. 10(*a*)], the first stage (*a*) shows the most critical microcrack stabilized by bridging fibers at a stress level below σ_{pc}, and with maximum crack opening δ_A smaller than δ^*. The second stage (*b*) shows the same crack with maximum crack opening δ_B beyond δ^*, and with remote load at the

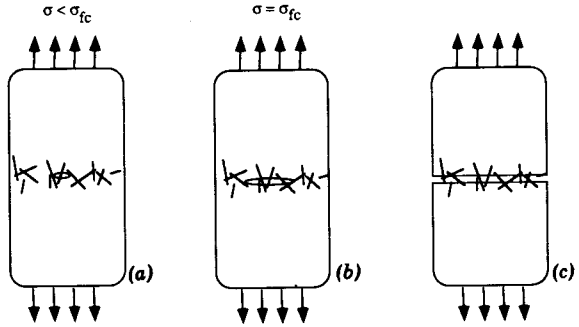

FIG. 9. Three Stages of Progressive Tensile Failure, Corresponding to (a) Microcrack Stabilized by Fiber Bridging at Load below First Crack Strength; and (b) Crack Becomes Unstable at First Crack Strength; and (c) Postmatrix Cracking with Load Carried Completely by Fibers Only

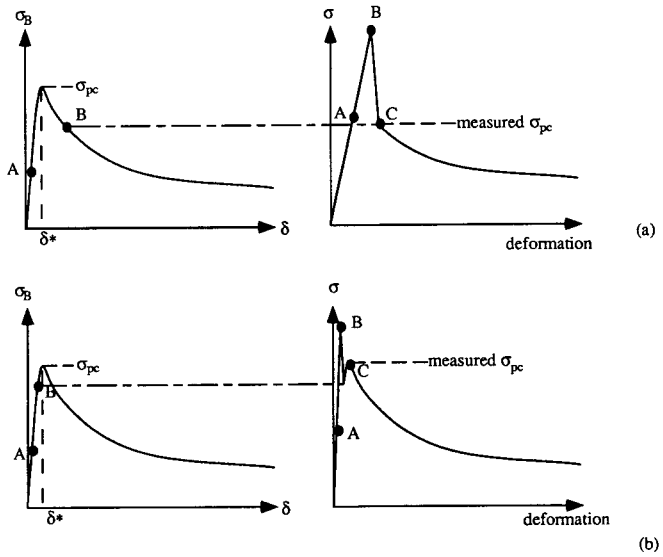

FIG. 10. Three Stages of Failure Indicated in Fig. 9 and Their Corresponding σ_B-δ Curve and Remote Load-Deformation Curves for Composite with (a) First Crack Strength Higher than σ_{pc} and $\delta_B > \delta^*$ and (b) First Crack Strength Lower than σ_{pc} and $\delta_B < \delta^*$

first crack strength, this crack grows indefinitely across the complete cross section of the specimen. This is presumably accompanied by the crack flattening out to a uniform opening at $\delta_C = \delta_B$, resulting in the postcrack configuration, stage (c). Subsequently, the measured composite stress-deformation relationship traces the pullout portion of the bridging stress-displacement curve. This scenario suggests that the measured postcrack strength could represent a lower bound of the true value, i.e., the peak of

the σ_B-δ curve. In the second scenario [Fig. 10(b)], the microcrack becomes unstable at stage (b), with $\delta_B < \delta^*$, and followed immediately by first cracking. In this case the postcracking part of the composite stress-deformation curve will trace part of the ascending branch and the complete descending pullout branch of the bridging stress-displacement curve, and the true peak of the σ_B-δ curve (at $\delta_C > \delta_B$) will be revealed. A more detailed discussion of possible tensile failure modes in fiber reinforced cementitious composites is given in Li and Leung (1991).

If the measured stress-deformation curve is as depicted in Fig. 10(a), as is most likely the case in the steel FRCC with low fiber volume fraction ($<2\%$), care must be taken in the interpretation of the postcracking strength. If the measured value underestimates the true value of σ_{pc} for the steel FRCC, it would mean that the value of f would be even larger than 1 as discussed previously in relation to Fig. 4.

Other sources of errors in the previous results and data interpretation include fiber/matrix interaction mechanisms not accounted for in the present analysis. These include fiber plastic bending, matrix spalling, and slip-dependent fiber/matrix interface shear resistance. In spite of these shortcomings, the scaling laws proposed in this paper presumably incorporate the major features of the physics of fiber bridging and are probably adequate for use in the engineering design of tensile properties of FRCC.

ACKNOWLEDGMENT

This research has been supported with grants to the University of Michigan, Ann Arbor, from the Air Force Office of Sponsored Research (Program Manager: Spencer Wu), and from the National Science Foundation (Program Manager: Ken Chong). The writer thanks C. K. Y. Leung and Y. Wang for many helpful discussions.

APPENDIX I. JUSTIFICATION OF APPROXIMATE ANALYSIS OF PULLOUT OF A SINGLE FIBER

For the problem of an elastic fiber embedded in a stiff matrix and pulled with an axial force P at its end $x = \ell$, where ℓ is the embedded length, the slippage $s(x)$, axial strain $\varepsilon(x)$, and axial force $F(x)$ at any point x along the length of the fiber is governed by

$$s(x) = s(0) + \int_0^x \varepsilon(x')\, dx' \quad \ldots\ldots (15)$$

$$\varepsilon(x) = \frac{4}{\pi d_f^2 E_f} F(x) \quad \ldots\ldots (16)$$

$$F(x) = \int_0^x \pi\tau d_f [1 + \varepsilon(x')]\, dx' \quad \ldots\ldots (17)$$

where $F(x = \ell) = P$; and x is measured from the embedded end of the fiber. These equations may be solved to obtain the peak load (when full debonding occurs)

$$P_{\text{peak}} = \frac{1}{4}\pi d_f^2 E_f \left[\exp\left(\frac{4\tau\ell}{d_f E_f}\right) - 1\right] \quad \ldots\ldots (18)$$

the displacement of the loaded end at peak load

$$\delta_{peak} = \frac{d_f E_f}{4\tau}\left[\exp\left(\frac{4\tau\ell}{d_f E_f}\right) - 1\right] - \ell \quad \ldots\ldots (19)$$

and the axial strain

$$\varepsilon(x) = \exp\left(\frac{4\tau\ell}{d_f E_f}\frac{x}{\ell}\right) - 1 \quad \ldots\ldots (20)$$

For $(\ell/d_f)/(E_f/\tau) \ll 1$, the axial strain may be linearized and the load P and displacement δ can then be related through (1). Because (E_f/τ) is typically two to three orders of magnitude larger than (ℓ/d_f) for discontinuous fibers, the error introduced by this linearization process is typically less than 1%. In arriving at (1), it should be noted that the elasticity of the matrix is ignored in favor of the deformability of the fiber. This is strictly correct only in the case of low fiber volume fraction and moderate elastic contrast between fiber and matrix moduli. These assumptions are generally reasonable for most fiber reinforced concrete.

Appendix II. Derivation of Prepeak Stress-Displacement Relation (5)

When normalized by σ_0, (4) may be rewritten in the form

$$\tilde{\sigma}_B(\delta) = \frac{8}{\pi\tau\left(\frac{L_f}{d_f}\right)d_f^2}\int_{\phi=0}^{\pi/2}\int_{z'=0}^{\cos\phi} P(\delta)\sin\phi\, dz'\, d\phi \quad \ldots\ldots (21)$$

where $z' \equiv z/(L_f/2)$. For the prepeak stress-displacement curve (i.e., $\delta < \delta^*$), there are two contributions from individual fibers (see Fig. 1). For those fibers located or oriented in such a way as to have a long embedded length ℓ, their major contributions are through fiber debonding, as described by (1). For the other fibers, their major contributions are through fiber slippage, as described by (2). Fibers in the first group passes into the second group as δ increases. For the first group of fibers, it is important to recognize that (1) holds as long as

$$\delta < \delta_0 \equiv \frac{2\ell^2\tau}{E_f d_f} = \frac{2\tau}{E_f d_f}\left(\frac{L_f}{2} - \frac{z}{\cos\phi}\right)^2 \quad \ldots\ldots (22)$$

where the embedded length ℓ has been re-expressed in terms of the fiber length L_f, the centroidal location z, and orientation ϕ of the particular fiber. After transformation and normalization, this becomes

$$z' < z_0\cos\phi \quad \ldots\ldots (23)$$

where

$$z_0 \equiv 1 - \left[\left(\frac{E_f}{\tau}\right)\left(\frac{d_f}{L_f}\right)\tilde{\delta}\right]^{1/2} \quad \ldots\ldots (24)$$

Thus, for this group of fibers, the contribution to the bridging stress is given by

$$\tilde{\sigma}_B(\delta)|_{debond} = \frac{8}{\pi\tau\left(\frac{L_f}{d_f}\right)d_f^2}\int_{\phi=0}^{\pi/2}\int_{z'=0}^{z_0\cos\phi} P(\delta)\sin\phi\, dz'\, d\phi \quad \ldots\ldots (25)$$

with $P(\delta)$ given by (1). The upper integration limit for z' in (25) ensures that only those fibers not fully debonded are counted in this contribution.

For the second group of fibers, slippage occurs, and (2) holds as long as

$$\delta_0 < \delta \le \ell = \left(\frac{L_f}{2} - \frac{z}{\cos\phi}\right) \quad \ldots\ldots (26)$$

or

$$z_0\cos\phi < z' \le (1 - \delta)\cos\phi \quad \ldots\ldots (27)$$

Thus for this group of fibers, the contribution to the bridging stress is given by

$$\tilde{\sigma}_B(\delta)|_{slipping} = \frac{8}{\pi\tau\left(\frac{L_f}{d_f}\right)d_f^2}\int_{\phi=0}^{\pi/2}\int_{z'=z_0\cos\phi}^{(1-\tilde{\delta})\cos\phi} P(\delta)\sin\phi\, dz'\, d\phi \quad \ldots\ldots (28)$$

with $P(\delta)$ given by (2). The lower integration limit for z' in (28) ensures that only those fibers fully debonded are counted in this contribution, and the upper integration limit ensures that those fibers that have fully slipped out of the matrix play no further role in the bridging stress.

By combining these two contributions by any given $\delta < \delta^*$, i.e.

$$\tilde{\sigma}_B(\tilde{\delta}) = \tilde{\sigma}_B(\tilde{\delta})|_{debond} + \tilde{\sigma}_B(\tilde{\delta})|_{slipping} \quad \ldots\ldots (29)$$

we obtain

$$\tilde{\sigma}_B(\tilde{\delta}) = g\left[\tilde{\delta}^2 - \frac{2}{3}\tilde{\delta}^*\tilde{\delta}^3 + 2\left(\frac{\tilde{\delta}}{\tilde{\delta}^*}\right)^{1/2} - \frac{4}{3}\left(\frac{\tilde{\delta}^3}{\tilde{\delta}^*}\right)^{1/2} - \frac{\tilde{\delta}}{\tilde{\delta}^*}\right] \quad \text{for } \tilde{\delta} \le \tilde{\delta}^* \quad \ldots\ldots (30)$$

and, for $\tilde{\delta}^* \ll 1$, the bridging stress-displacement relationship can be reduced to the simplified form in (5).

Appendix III. Derivation of Postpeak Stress-Displacement Relation (7)

We recognize that for $\delta > \delta^*$, all fibers would be slipping. Again, starting from (4), or (21), and eliminating all fibers that have fully slipped out from the matrix, the bridging stress may be written as

$$\tilde{\sigma}_B(\delta) = \frac{8}{\pi\tau\left(\frac{L_f}{d_f}\right)d_f^2}\int_{\phi=0}^{\pi/2}\int_{z'=0}^{(1-\tilde{\delta})\cos\phi} P(\delta)\sin\phi\, dz'\, d\phi \quad \ldots\ldots (31)$$

where the fiber bridging force is given by (2). Evaluation of this integral gives

$$\tilde{\sigma}_B(\tilde{\delta}) = g\left[(1-\tilde{\delta})^2 + \frac{2}{3}\tilde{\delta}^*(1-\tilde{\delta}_3)\right] \quad \ldots\ldots\ldots\ldots\ldots\ldots\ldots\ldots\ldots (32)$$

Because $\tilde{\delta}^* << 1$, the second term may be dropped without loss of accuracy, and (7) results.

APPENDIX IV. REFERENCES

Aveston, J., Cooper, G. A., and Kelly, A. (1971). "Single and multiple fracture." *Proc. of NPL Conference on the Properties of Fiber Composites,* National Physical Laboratory, London, England, 15–26.

Aveston, J., Mercer, R. A., and Sillwood, J. M. (1974). "Fiber reinforced cements—Scientific foundations for specifications." *Composites Standards Testing and Design, Conf. Proc.,* National Physical Laboratory, IPC Science and Technology Press, 93–103.

Bache, H. H. (1987). "Compact reinforced composite basic principles." *CBL Report No. 41,* Aalborg Portland Cement and Concrete Lab., Aalborg, Denmark.

Bentur, A., and Mindess, S. (1990). *Fiber reinforced cementitious composites.* Elsevier Appl. Sci., London, England.

Cooper, G. A., and Kelley, A. (1970). *Mechanics of composite materials.* F. W. Wendt, H. Liebowitiz, and N. Perrone, eds., Pergamon Press, Oxford, England, 653–661.

Cotterell, B., and Mai, Y-W. (1988). "Modelling crack growth in fiber-reinforced cementitious materials." *Material Forum,* 11, 341–351.

Krenchel, H., and Stang, H. (1989). "Stable microcracking in cementitious materials." *2nd Int. Symp. on Brittle Matrix Composites—BMC 2,* Polish Academy of Science, Cedzyna, Poland.

Li, V. C. (1990). "The effect of snubbing friction on the first crack strength of flexible fiber reinforced composites." *Proc. of the 8th European Congress of Fracture: Fracture Behavior and Design of Materials and Struct.,* European Group of Fracture, II, 738–745.

Li, V. C., and Leung, C. K. Y. (1991). "Tensile failure modes of random discontinuous fiber reinforced brittle matrix composites." *Fracture processes in concrete, rock and ceramics,* Chapman and Hall, U.K., 285–294.

Li, V. C., Wang, Y., and Backer, S. (1990). "Effect of inclining angle, bundling, and surface treatment on synthetic fiber pull-out from a cement matrix." *Composites,* 21(2), 132–140.

Li, V. C., Wang, Y., and Backer S. (1991). "A micromechanical model of tension-softening and bridging toughening of short random fiber reinforced brittle matrix composites." *J. of Mech. and Physics of Solids,* 39(5), 607–625.

Li, V. C., and Ward, R. (1989). "A novel testing technique for post-peak tensile behavior of cementitious materials." *Fracture Toughness and Fracture Energy,* Mihashi et al., eds., Balkema Press, Rotterdam, 183–195.

Morton, J., and Groves, G. W. (1976). "The effect of metal wires on the fracture of a brittle matrix composite." *J. of Materials Sci.,* 11, 617–622.

Naaman, A. E., Moavenzadeh, F., and McGarry, F. J. (1974). "Probabilistic analysis of fiber reinforced concrete." *J. of Engrg. Mech.,* ASCE, 100, 397–413.

Shah, S. P. (1990). "Toughening of quasi-brittle materials due to fiber reinforcing." *Micromechanics of failure of quasi-brittle materials,* S. P. Shah, S. E. Swartz, and M. L. Wang, eds., Elsevier Appl. Sci., Essex, England, 1–11.

Shah, S. P., Stroeven, P., Dalhuisen, D., van Stekelengerg, P. (1978). *RILEM Symp. Testing and Test Methods of Fiber Cement Composites,* The Construction Press, Lancaster, England, 399.

Visalvanich, K., and Naaman, A. E. (1982). "Fracture modelling for fiber reinforced cementitious composites." *Program Report for NSF Grant ENG 77-23534,* Dept. of Materials Engrg., Univ. of Illinois at Chicago Circle, Chicago, Ill.

Wang, Y., V. C. Li, and Backer, S. (1990). "Tensile properties of synthetic fiber reinforced mortar." *J. Cement and Concrete Composites,* 12(1), 29–40.

Wecharatana, M., and Shah, S. P. (1983). "A model for predicting fracture resistance of fiber reinforced concrete." *Cement and Concrete Res.,* 13. 819–829.